Evaluation of different approaches used to study membrane permeabilization by actinoporins on model lipid vesicles

Juan Palacios-Ortega[1,2], Esperanza Rivera-de-Torre[1,2], José G. Gavilanes[1], J. Peter Slotte[2,*] and Álvaro Martínez-del-Pozo[1,*]

[1]Departamento de Bioquímica y Biología Molecular, Universidad Complutense, Madrid, Spain

[2]Biochemistry, Faculty of Science and Engineering, Åbo Akademi University, Turku, Finland

ABSTRACT

Release of aqueous contents from model lipid vesicles has been a standard procedure to evaluate pore formation efficiency by actinoporins, such as sticholysin II (StnII), for the last few decades. However, regardless of the probe of choice, the results reported that StnII action was never able to empty the vesicles completely. This was hard to explain if StnII pores were to be stable and always leaky for the probes used. To address this question, we have used a variety of probes, including rhodamine 6G or Tb^{3+}, to test the permeability of StnII's pores. Our results indicate that calcein was in fact too large to fit through StnII's pores, and that the standard method in the field is actually reporting StnII-induced transient permeation of the membrane rather than the passage of solutes through the stable assembled pores. In order to evaluate the permeability of these structures, we used a dithionite-based assay, which showed that the final pores were in fact open. Thus, our results indicate that the stable actinoporins' pores are open in spite of plateaued classic release curves. Besides the proper pore, the first stages of pore formation would inflict serious damage to living cells as well.

KEYWORDS

Pore-forming-proteins, leakage, calcein, rhodamine, terbium, NBD-dithionite.

ABBREVIATIONS

$C_{12}E_8$, Octaethylene glycol monododecyl ether; Chol, Cholesterol; DOPC, 1,2-dioleoyl-sn-glycero-3-phosphocholine; eSM, egg sphingomyelin; LUV, large unilamelar vesicle; POPE-NBD, 1,2-dioleoyl-sn-glycero-3-phosphoethanolamine-N-(7-nitro-2-1,3-benzoxadiazol-4-yl); SM, sphingomyelin; Stn, sticholysin.

1. Introduction

Sea anemone actinoporins represent an optimal system to study the transition from a water-soluble monomeric protein conformation to an oligomeric transmembrane pore [1-3]. These pore-forming toxins constitute multigenic families that have been detected in many sea anemone species [3-7]. However, only four of them have been characterized in detail: Sticholysins I and II (StnI and StnII, respectively) from *Stichodactyla helianthus* [1-3], equinatoxin II from *Actinia equina* [4, 8], and fragaceatoxin C from *Actinia fragacea* [9]. All show almost identical monomeric water-soluble three-dimensional structure composed of a β-sandwich motif flanked by two α-helices [10-15]. One of these helices, located at the N-terminal end, is responsible for the actual formation of the pore penetrating the membrane [16-22]. The incorporation of these proteins to the bilayer depends largely on the lipid composition and the physicochemical properties of the membrane [8, 20, 23-31]. Sphingomyelin (SM) is required [26, 32-34], but other factors, such as the presence of sterols, the coexistence of various phases or domains, lateral packing, fluidity, membrane thickness, and the strength of the SM interfacial hydrogen bonding network, have a strong influence on the pore-forming ability of these proteins [20, 26, 28-31, 34-47].

Almost forty years have passed since it was demonstrated, using different K^+ or Ca^{2+} containing solutions, that these proteins form cation-selective pores at neutral pH [23, 35, 48-52]. Altogether, those studies evidenced that actinoporins increase cell membrane permeability for monovalent and divalent cations. Only a few years later, these pores were also characterized using different electrophysiological approaches, including the use of lipid planar membranes. These studies confirmed their specificity for cations and revealed a pore size in the order of 1-2 nm of radius [16, 49-52]. In fact, the only two available crystalline structures of actinoporin pores fit rather well within this size range (Fig. 1) [13, 15]. Interestingly, despite the specificity of the pore for cations, most researchers in the field, including us, have been using negatively charged fluorophores, such as calcein or carboxyfluorescein, as the main probes to explore the molecular features of these pores. In this work, we challenge this approach and suggest a more sensitive procedure to study the pore-forming mechanism of these intriguing metamorphic proteins.

2. Materials and methods

2.1. Materials

Calcein, Rhodamine 6G, terbium chloride, dextran-labelled fluorescein, Triton X-100 and octaethylene glycol monododecyl ether (C12E8) were obtained from Sigma-Aldrich (St. Louis, MO). Cholesterol (Chol), egg sphingomyelin (eSM), 1,2-dioleoyl-sn-glycero-3-phosphocholine (DOPC), and 1,2-dioleoyl-sn-glycero-3-phosphoethanolamine-N-(7-nitro-2-1,3-benzoxadiazol-4-yl) (POPE-NBD) were from Avanti Polar Lipids (Alabaster, AL). StnII was produced in *Escherichia coli* RB791 and purified to homogeneity as described in [53].

2.2. Preparation of vesicles

Briefly, large unilamelar vesicles (LUVs) were made by extruding resuspended DOPC:eSM:Chol (1:1:1) dried lipid films as previously described [20-22, 30]. This

composition is the standard used in the actinoporin field, providing both recognition targets (SM) as well as the most appropriate physicochemical properties [20, 22, 30, 31, 37, 38, 42, 43, 45, 47, 54]. Lipid films were made from a methanol mixture of the desired lipids dried under nitrogen flow. This film was later kept under vacuum for at least two hours to ensure complete elimination of the organic solvent. Specific details for each set of pore-forming experiments are provided in the following sections. In all cases, when measuring the release of encapsulated solutes (see below) and in order to ensure that no spontaneous leakage occurred, fluorescence emission was recorded for 5 min before toxin addition. A steady signal level, indicating intact vesicles, was observed for all samples and experiments described below.

2.3. Calcein Release

Calcein-entrapped LUVs were prepared by extrusion through 200 nm filters at 60 °C [20-22, 30, 34, 47]. Tris buffer (10 mM Tris, 140 mM NaCl, pH 7.4) containing calcein at 100 mM was employed. LUVs were separated from non-entrapped calcein by gel filtration on Sephacryl S200HR [20-22, 30, 34] and then used for permeabilization studies within 8 h of preparation. LUVs lipid concentration was 0.25 – 0.5 mM before extrusion. Lipid concentration during the calcein leakage experiments was 2.5 μM. The volume of the samples was 2.0 mL. Emission at 550 nm (emission at the 505 nm maximum was high enough as to damage the spectrofluorimeter's photomultipliers) was followed at 23 °C as a function of time (λ_{ex} = 480 nm). Fluorescence emission was measured in a PTI Quanta-Master spectrofluorimeter (Photon Technology International, Inc., Birmingham, NJ, USA). Fraction of calcein released was determined based on maximum calcein release induced by LUV disintegration using 10 μL of 10 % v/v Triton X-100.

2.4. Rhodamine 6G Release

Rhodamine 6G (R6G) was fist diluted in distilled water to saturation. A 5x aliquot of the Tris buffer, detailed in the previous paragraph, was added to the R6G solution. R6G precipitate was removed by centrifugation. R6G concentration in encapsulation buffer was then approximately 5 mM. LUVs were again used for permeabilization studies within 8h. Lipid concentration was the same as for calcein assays. Emission was followed at 555 nm at 23 ºC as a function of time, using 525 nm excitation. Maximum release was obtained by LUVs disintegration using 10 μL of 20 mM $C_{12}E_8$. Triton X-100 was not used because it quenched R6G emission.

2.5. Terbium Release

Terbium release experiments were performed using a standard protocol [55, 56], with minor adaptations regarding lipid concentrations. HEPES buffer was used instead of TES. Vesicles were extruded through 400 nm filters to increase the amount of cation encapsulation and therefore increasing the sensitivity of the subsequent measurements. Fluorescence emission was recorded at 545 nm, using 270 nm excitation. Terbium must be chelated in order to remain soluble [57]. Thus, it was encapsulated chelated with citrate, with which it forms a very weakly fluorescent complex. Upon membrane permeabilization, and subsequent release, citrate is easily displaced from the complex by the impermeant aromatic chelator dipicolinic acid (DPA), located outside of the

vesicles (Fig. 4). The assay is based on recording the fluorescence increase by the interaction established between the Tb^{3+} released from the interior of the vesicles and DPA. The enhancement of terbium fluorescence by DPA is due to energy transfer from its aromatic ring. Due to inner filter effects, the use of Triton X-100 had to be avoided. Instead, reduced Triton X-100, which lacks the absorption band at 270 nm, was employed. Protein absorption at 270 nm was negligible at the protein concentrations assayed.

2.6. Proton Release

Proton release from LUVs was measured monitoring the change in fluorescence emission of fluorescein. Fluorescein absorption spectra undergoes a significant change upon pH increase, with a new absorption maximum appearing at 488 nm, thus increasing absorption and, consequently, emission if excited at that wavelength. StnII activity should allow for proton efflux and consequent pH increase inside the vesicle. Fluorescein coupled to 3000 Da dextran was used to avoid fluorescein release from LUVs. The fluorescein-dextran complex was encapsulated at a concentration of 5 µM. The buffer was 10 mM sodium phosphate. pH was set to 4.2 inside of the LUVs, while the pH outside was kept at 7.2. Emission was recorded at 520 nm. Maximum emission was again obtained using Triton X-100 as in the calcein assays.

2.7. Peptide-induced membrane perturbation models

Experimental data from the leakage experiments were fitted by the following model:

$$\frac{F_{obs}(t)}{F_{max}} = 1 - \exp(J_2(e^{-\nu_{relax}t} - 1)) \qquad \text{(eq. 1)}$$

as defined by Andersson *et al.* [58]. Briefly, the model describes release curves produced by the release of aqueous contents induced by transient perturbations affecting the membrane. Once the system reached equilibrium, the perturbations cease and leakage is no more, regardless of the probe concentration in the inside and outside compartments. Here on, this model will be referred to as the perturbation model.

The model has two parameters. J_2 is proportional to the magnitude of the perturbations and, if the model fits nicely the experimental data, it can be obtained straight from $J_2 = 1 - \ln|1 - L_{max}|$, where L_{max} is the value of the final, maximum release. ν_{relax} is related to the lifetime of the perturbations. It can be shown that the product $J_2 \cdot \nu_{relax}$ is equal to the slope of the release curves at $t = 0$.

2.8. Equilibrium pore assay

In order to evaluate transient non-equilibrium leakage phenomena, a modification of a previously described method was employed [56]. DOPC:eSM:Chol (1:1:1) LUVs containing 1 mol% of POPE-NBD were prepared. A freshly prepared solution of 0.6 M sodium dithionite in 1.0 M sodium phosphate buffer, pH 10, was employed to quench the emission of the NBD in the outer leaflet. The experiments were performed by recording the fluorescence emission at 520 nm, using an excitation wavelength of 470 nm. Two different types of experiments were performed. In the first set of measurements, the vesicles were first incubated with different StnII

concentrations for 90 s and then dithionite was added to final concentration of 55 mM. When a steady fluorescence emission signal was obtained, Triton X-100 was used as describe above to disintegrate the vesicles. The total drop in fluorescence was considered as the maximum effect exerted by dithionite, corresponding to reduction of all NBD molecules present in the sample. In the second set of experiments, dithionite was added first. This produced a fluorescence drop of about 50%, corresponding to reduction of POPE-NBD molecules on the outer layer of the membrane. Then, StnII was added and fluorescence was further recorded. As in the first set of experiments, vesicles were also disintegrated with Triton X-100 once reached a steady signal was reached.

3. Results

3.1. Calcein leakage

The initial aim of this study was to assess the suitability of the calcein-release approach, a well-established assay for evaluating the pore forming ability of actinoporins [20-22, 24, 25, 27, 30, 31, 47, 51, 52, 59-61]. We used StnII, which has been thoroughly characterized previously, to compare the efficacy of the different approaches to the calcein release assay [20-22, 30, 31, 43, 45, 47]. Calcein release experiments yielded the results shown in Fig. 2. Thus, incubation of calcein-entrapped vesicles with StnII at different protein/lipid ratios reached a plateau representing the release of only about 60% of the total fluorophore contained into the vesicles (Fig. 2A). The LC_{50} value, defined as the concentration of protein needed to obtain a final release of 50% of the maximum protein-induced release, was 52 pM (Table 1).

Most standard methods used to analyze actinoporin-induced calcein release usually rely on recording the percentage of fluorophore leaked, as calculated based on total fluorescence intensities, after a fixed amount of time. This methodological approach can artificially reduce the observed differences when using high actinoporin concentrations [31]. Thus, the maximum rate values of fluorophore release were also quantitated for the different protein/lipid ratios employed. These second set of results, shown in Fig. 2B, can be considered to represent a much more valuable parameter, containing information about both kinetic and dye-release proficiency. Considering the calcein-leakage experiments, the maximum release rate obtained at saturating concentrations of StnII (20 nM protein concentration, corresponding to a protein/lipid molar ratio of 8×10^{-3}) was 0.061 ΔF units/s (Table 1).

3.2. Rhodamine 6G leakage

Rhodamine 6G release rate (Fig. 2) was almost four-fold faster than the value obtained for calcein leakage (Table 1) at the mentioned saturating protein/lipid ratio of 8×10^{-3}. Accordingly, the LC_{50} value was also in the order of six-fold lower (Table 1). Quite unexpectedly, however, the final plateau of maximum fluorophore release did correspond again to only about 60% of the originally encapsulated probe (Fig. 2A). R6G was released much faster but the final percentage of probe release was essentially identical to the value found for calcein.

3.3. Cation (Tb^{3+} or H^{+}) leakage

In order to assess the ability of small cations to go through the actinoporins pore, two different assays were performed. First, the permeability of StnII pores to the lanthanide Tb^{3+} was tested. Second, we assessed the possibility of protons crossing the pore by recording the pH-sensitive emission of an encapsulated dextran-fluorescein derivative.

In both cases, very poor release values were observed, not only in kinetic terms but also considering the final release of the contents, measured at saturating concentrations (Fig. 2 and Table 1). Final release never exceeded 60 %, as for the previous assays (Fig. 2A). In this case, the LC_{50} values were 1.99 and 2.88 nM for Tb^{3+} and H^+, respectively. These values were larger than those obtained for calcein or R6G release experiments. The maximum rate value of Tb^{3+} release for saturating StnII protein/lipid ratio was even lower than the value obtained for calcein (Table 1). Proton leakage was much faster (Table 1) but only at very high protein concentration (Fig. 3B). In fact, the corresponding curve was highly cooperative (Fig. 3B) probably reflecting the protonation of some key residues located at the lumen of the pore (see Discussion).

3.4. Kinetic and protein concentration-dependence modeling

The perturbation model [58] was used to evaluate the experimental leakage data. For all four types of reporters employed (calcein, R6G, Tb^{3+}:citrate, and H^+-fluorescein) the model provided very good fits (Figure S1), indicating the consistency of the data with the theoretical basis of the model.

3.5. Equilibrium pore assays

Transient permeabilization refers to the disruption of bilayer integrity while subjected to the action of a pore forming polypeptide. In all previous assays, protein-membrane interaction took place when the tracing molecules *had already* been encapsulated. Thus, those assays cannot differentiate transient permeabilization from actual flux through the pore. With the aim of discerning the influence of this potential transient permeabilization on the rate and efficiency of actinoporins pore-formation, different experiments were performed using DOPC:eSM:Chol (1:1:1) LUVs containing 1 mol% of POPE-NBD (Fig. 3). NBD was quenched using sodium dithionite, which can be added to the sample both *before* or *after* protein-membrane interaction takes place. This way, actual flux through the pore, ruling out influence of transient permeabilization, can be measured.

As shown in Fig. 4A, incubation of NBD-labeled vesicles with sodium dithionite produced around a 40% decrease of the NBD fluorescence emission at 520 nm. This result not only confirmed the availability to the reducing agent of most of the NBD located at the outer leaflet but also the impermeability of the intact membrane to the reducing agent (at these short time frames). In good agreement with this hypothesis, lysis of the membranes with Triton X-100 was enough to quench the remaining 60% NBD-emission. Theoretically, the fluorescence drop should be more similar and quite close to 50% in both cases. However, Triton X-100 produces a distortion in NBD fluorescence, which has not been discounted in the raw experiments shown in Fig. 3.

In a second set of experiments, these vesicles were incubated with increasing concentrations of StnII for long enough to assume the formation of stable protein pores.

Interestingly, the subsequent addition of dithionite resulted in an almost complete quenching of all fluorescence emission, of very similar magnitude as the Triton X-100 addition in the first experiment described. Consequently, further addition of this detergent to the samples only produced a small effect on the intensity of the emission (Fig. 3B).

The third series of experiments was carried out reversing the order of the reagents involved. The vesicles were first incubated with dithionite, which yielded the already observed fluorescence decrease of ~40 % (Fig. 3A and C). Once a stable signal was reached, the protein was then added, again in increasing concentrations. When the amount of protein was large enough to exert a saturating effect, the fluorescence was extinguished for a further 40%. The subsequent addition of Triton X-100 produced quenching of the remaining 20% fluorescence emission. This final effect is most likely a consequence of to the aforementioned effect of Triton X-100 on NBD emission.

Considering these sets of experiments, it could be concluded that, independently of the presumable transient permeability of some pore intermediates, an equilibrium was finally reached and the final stable StnII pores were permeable to the dithionite anion ($S_2O_4^{2-}$).

4. Discussion

The very first articles in which the cation-specificity and dimensions of actinoporin pores were established were mainly based on electrophysiological measurements. [23, 26, 35, 49, 50]. However, many of the later reports were obtained using bulkier experiments based on the employment of artificial lipid vesicles. These studies focused on deciphering the actinoporins' pore formation mechanism by means of measuring the release of encapsulated fluorophores, such as calcein [14, 20-22, 24, 25, 30, 31, 34, 42-45, 47, 54] or carboxyfluorescein [62-66]. This is however a striking remark, considering that not only calcein and carboxyfluorescein are negatively charged at the pH values employed in all those experiments, but that they also have hydrodynamic radii of about 0.74 [67] and 0.50 nm [68], respectively (Fig. 4 and Table 2). Those are smaller values than actinoporins' pore radius but quite close to the 1-2 nm values reported in the literature (Fig. 1) [12, 13, 15, 16, 26, 49-52, 69]. In fact, it was using liposomes encapsulating NADH (net charge of -2) and dextran FD-4 (0.6 nm and 1.2 nm Stokes radius, respectively) (Table 2) [70] that it was confirmed that StnII pores on SM-containing liposomes show a hydrodynamic pore size within the mentioned range. NADH leaked out of the vesicles, while FD-4 remained encapsulated under identical assay conditions [26], a result in good agreement with the dimensions later found in the most accepted actinoporin pore crystalline structure [15]. In this example, the actinoporin fragaceatoxin C, isolated using detergents, assembles into an octameric pore with an inner radius ranging between 3.0 nm at the upper vestibule side, and 0.8 nm at is narrowest constriction connected to the vesicle's lumen (Fig. 1). Therefore, though the actinoporins' pore seems to be selective for atomic cations, the calcein-release assay would rather measure the actinoporin-induced membrane permeability to negatively charged solutes of ~ 700 Da. These measurements would account mostly for StnII molecules destabilizing the membrane while assembling into the final oligomeric pore structures (see below).

R6G is a cationic water-soluble highly fluorescent probe (Fig. 2). Thus, it was initially considered as a better molecule to evaluate the actinoporins' pore forming ability. In good agreement with this working hypothesis, the R6G release rate was much faster. Its maximum value was about 3.7-fold higher at the saturating protein/lipid molar ratio of 8 x 10^{-3}, in comparison with the values obtained for calcein release experiments (Fig. 2 and Table 1). Therefore, as expected, the net charge of the fluorophore probe employed would be a key factor for membrane pore-mediated permeation by actinoporins. However, and quite intriguingly, in both types of assays final leakage at saturating protein concentrations was plateaued at only 60% of the fluorescence intensity, referred to the intensity obtained in the presence of a detergent concentration (Triton X-100 or $C_{12}E_8$) producing 100% of vesicle lysis. Taking into account the very similar size of R6G (hydrodynamic radius of about 0.59 nm, [71]; Table 2) and the negatively charged NADH, calcein, and carboxyfluorescein molecules (Fig. 4), these results suggest a pore-forming mechanism where membrane impermeability, regarding these molecules, would be initially compromised, but later restored, after reaching the final equilibrium of protein integration into the membrane. A mechanism suggesting that the initial leakage observed was not due to stable pore-formation but rather to the transient appearance of intermediates that compromise membrane integrity. This interpretation would also agree with several articles that have convincingly suggested the existence of different actinoporin protomer arrangements capable of transiently altering membrane permeability [18, 19, 69, 72-78]. According to this interpretation, once the final and thermodynamically stable pores are formed [15], neither calcein nor R6G would have the right size to keep on crossing the membrane through the pore lumen and, consequently, would remain within the vesicles. After all, the hydrodynamic ionic radii of Ca^{2+} and K^{+}, which are supposed to be the natural cations flowing through the actinoporins pore lumen [23, 35, 48-52], are only about 0.10 and 0.14 nm, respectively, much smaller than the radius estimated for calcein, carboxyfluorescein, or R6G (Table 2).

Smaller cations were also considered as potential probes for the study of actinoporins' pores. At first glance, the most obvious candidate was Tb^{3+}, which ionic radius is only ~0.12 nm, and emits light when chelated by DPA. Unfortunately, these experiments yielded very poor results in both kinetic and total final leakage terms (Fig. 2; Table 2). The easiest explanation resides in the fact that Tb^{3+} solubility in water is low and the assay is not feasible if Tb^{3+} is not chelated and solubilized by citrate. Tb^{3+} is chelated with two citrate ions, which each displays three negative charges, yielding Tb^{3+}:citrate complexes, which would have net charge of -3, and size much larger than expected (Fig. 4). The real situation would then be very similar to the one found with calcein or R6G: size would impede permeation thorough the pore lumen once the final thermodynamically stable structures are assembled. An alternative explanation would be that the assays cannot just be made with any atomic cation. At neutral pH, the channel seems to be quite specific. It has been described how Ni^{2+} can inhibit hemolysis exerted by equinatoxin II [50, 51], another well-known actinoporin. From this point of view, and regardless of the chelation with citrate, Tb^{3+} might have not been a good option either.

Leakage of protons can be monitored using a pH sensitive fluorescent probe bound to dextran of enough size as to be impermeable to the membrane

permeabilization by actinoporins. This approach was also considered worth trying since protons are the smallest possible cations. LUVs containing fluorescein coupled to 3000 Da dextran were used to perform a fourth set of leakage experiments. The pH value was set to 4.2 inside of the LUVs, while the pH outside was kept at 7.2. Unfortunately, leakage was very slow and only noticeable at the highest StnII concentrations assayed (Fig. 2). This could be explained taking into account that it has been described how above pH 7.0 the membranes containing actinoporins pores are highly specific for K^+, whereas below pH 4.0 they are poorly selective [35], being its maximum at pH values of 8.0-9.0 [51]. The pK_a value for the mentioned titratable groups was found to be 5.0 [35]. Therefore, the assay herein described would not be measuring directly the proton permeability of the pores but rather the pH influence on their ion selectivity.

Another consideration to be discussed would be how this cation selectivity and the observed rectification of the actinoporins' pore channel have been already interpreted as being a reflection of charges asymmetrically distributed along the pore [50]. Electrophysiological experiments performed by other authors with Ca^{2+} solutions yielded results that were interpreted as the Ca^{2+} cations screening negatively charged groups along the channel, most probably carboxylate groups [35]. These groups would be also asymmetrically distributed, closer to the "entrance" of the channel, the wider opening in Fig. 1. Accordingly, these groups were not titratable from the other side, the narrower one. In summary, cation passage through the channel is not symmetrical and the experiments employing model lipid vesicles would measure the less favorable flow of cations exiting the vesicles interior from the narrow to the wider opening, when the pores seem to be designed to perform the opposite function: allowing cations in.

Transient permeation refers to the interruption of bilayer integrity while subjected to a pore-forming polypeptide. In fact, many peptide-induced membrane permeation events occur through unbalanced transient processes [56, 79, 80]. In these examples, leakage occurs only in the minutes immediately after peptide addition. The system then relaxes to a state where leaking slows down, or stops completely, despite the presence of the polypeptides in the bilayer. This concept has been coined for small membrane-disturbing peptides, such as mellitin [80], for example, but in the view of the results shown here, it could be also applicable to actinoporins mechanism of action. In fact, the data was consistent with a previously published model that describes transient leakage through membrane perturbations [58], supporting our hypothesis.

This is a rather interesting conclusion, since the formation of transient pore conformations has been already described for actinoporins [8, 19]. Therefore, the question that remained was whether Stn-induced leakage was solely due to transient permeation, as appears to be when calcein or R6G are the probes employed, or if pores remained open to other substances with suitable features. These aspects were then studied through the equilibrium pore experiments described in Fig. 3.

In a first set of experiments, the vesicles were incubated with increasing concentrations of StnII for long enough as to assume the formation of stable protein pores. Then, the subsequent addition of dithionite resulted in almost complete quenching of all fluorescence emission, suggesting that NBD would be available to dithionite at both sides of the bilayer. The reverse set of experiments were also

performed as control. Dithionite was added first and, once it had reacted with all the NBD available at the outer lipid layer, increasing concentrations of StnII were added. Again, fluorescence quenching was complete, showing that the remaining reagent was also able to enter the vesicles. Altogether, all these experiments in Fig. 3 rather suggest that dithionite, a negatively charged but very small molecule, would be able to cross the channel of the actinoporins' pore. Even considering that the pores are cation-specific, size appears to be the key factor for allowing passage, at least when using assays based on the measurement of molecule release from model lipid vesicles.

5. Conclusion

In the light of the experiments reported so far in the literature, and our own results shown here, we conclude that size, rather than charge, would be the key factor for discriminating passage through actinoporins pore. This assertion does not contradict the well-established fact that it is a cation specific channel, especially in kinetic terms, considering the asymmetry of the cations flow through the channel. Leakage observed using model lipid vesicles and the archetypical fluorescent probes generally employed in the field would most likely only reflect transient instability of membrane impermeability, probably mediated by dynamic, not completely assembled, pore intermediates, and initiated by helix insertion in the membrane. These intermediates, however, are of great significance for the molecular mechanism conducing to the final and more thermodynamically stable assemblies of the still controversial structure of actinoporins' pore. In our opinion, calcein can still be used with this purpose, but results should be interpreted with caution in the light of the new evidences shown here. R6G can be a better probe in terms of sensitivity but, as calcein, is too big for actinoporin's pores. Formation of competent pores should be checked using the NBD-dithionite assay.

AUTHOR INFORMATION

Corresponding Authors

*Álvaro Martínez-del-Pozo, Departamento de Bioquímica y Biología Molecular, Universidad Complutense, 28040 Madrid, Spain. Tel: +34 91 394 4259. E-mail: alvaromp@quim.ucm.es, or J. Peter Slotte, Biochemistry, Faculty of Science and Engineering, Åbo Akademi University, 20520 Turku, Finland. Tel: +358 40 581 6521. E-mail: jpslotte@abo.fi

ORCID

Juan Palacios-Ortega: 0000-0002-4629-0221

Esperanza Rivera-de-Torre: 0000-0002-0272-6150

José G. Gavilanes: 0000-0002-6852-341X

J. Peter Slotte: 0000-0002-4850-5759

Álvaro Martínez-del-Pozo: 0000-0003-0043-5939

Author Contributions

JPO and ERT performed the experiments. All authors contributed to conceiving the project, designing the experiments, discussing and interpreting the results, and writing the manuscript.

Declaration of competing interest

The authors declare no competing financial interest.

Acknowledgements

This research was supported by the Sigrid Juselius Foundation, the Jane and Aatos Erkko Foundation, and the Magnus Ehrnrooth Foundation (to J.P.S.), and by UCM-Banco Santander grant PR75/18-21561 (to A.M.-d.-P.). J.P.-O. has a funded doctoral student position from ISB/ÅA. UCM-Banco Santander fellowship was granted to E.R.-d.-T.

References

[1] J. Alegre-Cebollada, M. Oñaderra, J.G. Gavilanes, A. Martínez-del-Pozo, Sea anemone actinoporins: The transition from a folded soluble state to a functionally active membrane-bound oligomeric pore, Curr Protein Pept Sci, 8 (2007) 558-572.

[2] L. García-Ortega, J. Alegre-Cebollada, S. García-Linares, M. Bruix, A. Martínez-del-Pozo, J.G. Gavilanes, The behavior of sea anemone actinoporins at the water-membrane interface, Biochim Biophys Acta, 1808 (2011) 2275-2288.

[3] S. García-Linares, E. Rivera-de-Torre, J. Palacios-Ortega, J.G. Gavilanes, A. Martínez-del-Pozo, The metamorphic transformation of a water-soluble monomeric protein into an oligomeric transmembrane pore, in: A. Iglič, M. Rappolt, A.J. García-Sáez (Eds.) Advances in Biomembranes and Lipid Self-Assembly, vol. 26, 2017, pp. 51-97.

[4] G. Anderluh, I. Krizaj, B. Strukelj, F. Gubensek, P. Maček, J. Pungercar, Equinatoxins, pore-forming proteins from the sea anemone *Actinia equina*, belong to a multigene family, Toxicon, 37 (1999) 1391-1401.

[5] E.V. Leychenko, M. Isaeva, E. Tkacheva, E. Zelepuga, A. Kvetkina, K. Guzev, M. Monastyrnaya, E. Kozlovskaya, Multigene Family of Pore-Forming Toxins from Sea Anemone *Heteractis crispa*, Mar Drugs, 16 (2018) 183.

[6] E. Rivera-de-Torre, A. Martínez-del-Pozo, J.E. Garb, *Stichodactyla helianthus*' de novo transcriptome assembly: Discovery of a new actinoporin isoform, Toxicon, 150 (2018) 105-114.

[7] E. Rivera-de-Torre, J. Palacios-Ortega, J.G. Gavilanes, A. Martínez-del-Pozo, S. García-Linares, Pore-Forming Proteins from Cnidarians and Arachnids as Potential Biotechnological Tools, Toxins (Basel), 11 (2019).

[8] N. Rojko, M. Dalla Serra, P. Maček, G. Anderluh, Pore formation by actinoporins, cytolysins from sea anemones, Biochim Biophys Acta, 1858 (2016) 446-456.

[9] A. Bellomio, K. Morante, A. Barlič, I. Gutiérrez-Aguirre, A.R. Viguera, J.M. González-Mañas, Purification, cloning and characterization of fragaceatoxin C, a novel actinoporin from the sea anemone *Actinia fragacea*, Toxicon, 54 (2009) 869-880.

[10] A. Athanasiadis, G. Anderluh, P. Maček, D. Turk, Crystal structure of the soluble form of equinatoxin II, a pore-forming toxin from the sea anemone *Actinia equina*, Structure, 9 (2001) 341-346.

[11] M.G. Hinds, W. Zhang, G. Anderluh, P.E. Hansen, R.S. Norton, Solution structure of the eukaryotic pore-forming cytolysin equinatoxin II: Implications for pore formation, J Mol Biol, 315 (2002) 1219-1229.

[12] J.M. Mancheño, J. Martín-Benito, M. Martínez-Ripoll, J.G. Gavilanes, J.A. Hermoso, Crystal and electron microscopy structures of sticholysin II actinoporin reveal insights into the mechanism of membrane pore formation, Structure, 11 (2003) 1319-1328.

[13] A.E. Mechaly, A. Bellomio, D. Gil-Carton, K. Morante, M. Valle, J.M. González-Mañas, D.M. Guerin, Structural insights into the oligomerization and architecture of eukaryotic membrane pore-forming toxins, Structure, 19 (2011) 181-191.

[14] S. García-Linares, I. Castrillo, M. Bruix, M. Menéndez, J. Alegre-Cebollada, A. Martínez-del-Pozo, J.G. Gavilanes, Three-dimensional structure of the actinoporin sticholysin I. Influence of long-distance effects on protein function, Arch Biochem Biophys, 532 (2013) 39-45.

[15] K. Tanaka, J.M. Caaveiro, K. Morante, J.M. González-Mañas, K. Tsumoto, Structural basis for self-assembly of a cytolytic pore lined by protein and lipid, Nat Commun, 6 (2015) 6337.

[16] P. Malovrh, G. Viero, M.D. Serra, Z. Podlesek, J.H. Lakey, P. Maček, G. Menestrina, G. Anderluh, A novel mechanism of pore formation: membrane penetration by the N-terminal amphipathic region of equinatoxin, J Biol Chem, 278 (2003) 22678-22685.

[17] I. Gutiérrez-Aguirre, A. Barlič, Z. Podlesek, P. Maček, G. Anderluh, J.M. González-Mañas, Membrane insertion of the N-terminal α-helix of equinatoxin II, a sea anemone cytolytic toxin, Biochem J, 384 (2004) 421-428.

[18] N. Rojko, K.C. Kristan, G. Viero, E. Zerovnik, P. Maček, M. Dalla Serra, G. Anderluh, Membrane damage by an α-helical pore-forming protein, Equinatoxin II, proceeds through a succession of ordered steps, J Biol Chem, 288 (2013) 23704-23715.

[19] V. Antonini, V. Perez-Barzaga, S. Bampi, D. Penton, D. Martinez, M. Dalla Serra, M. Tejuca, Functional Characterization of Sticholysin I and W111C Mutant Reveals the Sequence of the Actinoporin's Pore Assembly, PLoS One, 9 (2014) e110824.

[20] J. Palacios-Ortega, S. García-Linares, M. Astrand, M.A. Al Sazzad, J.G. Gavilanes, A. Martínez-del-Pozo, J.P. Slotte, Regulation of Sticholysin II-Induced Pore Formation by Lipid Bilayer Composition, Phase State, and Interfacial Properties, Langmuir, 32 (2016) 3476-3484.

[21] J. Palacios-Ortega, S. García-Linares, E. Rivera-de-Torre, J.G. Gavilanes, A. Martínez-del-Pozo, J.P. Slotte, Differential Effect of Bilayer Thickness on Sticholysin Activity, Langmuir, 33 (2017) 11018-11027.

[22] E. Rivera-de-Torre, J. Palacios-Ortega, S. García-Linares, J.G. Gavilanes, A. Martínez-del-Pozo, One single salt bridge explains the different cytolytic activities shown by actinoporins sticholysin I and II from the venom of *Stichodactyla helianthus*, Arch Biochem Biophys, 636 (2017) 79-89.

[23] M.L. Shin, D.W. Michaels, M.M. Mayer, Membrane damage by a toxin from the sea anemone *Stoichactis helianthus*. II. Effect of membrane lipid composition in a liposome system, Biochim Biophys Acta, 555 (1979) 79-88.

[24] G. Belmonte, C. Pederzolli, P. Maček, G. Menestrina, Pore formation by the sea anemone cytolysin equinatoxin-II in red blood cells and model lipid membranes, J Membr Biol, 131 (1993) 11-22.

[25] M. Tejuca, M.D. Serra, M. Ferreras, M.E. Lanio, G. Menestrina, Mechanism of membrane permeabilization by sticholysin I, a cytolysin isolated from the venom of the sea anemone *Stichodactyla helianthus*, Biochemistry, 35 (1996) 14947-14957.

[26] V. De los Ríos, J.M. Mancheño, M.E. Lanio, M. Oñaderra, J.G. Gavilanes, Mechanism of the leakage induced on lipid model membranes by the hemolytic protein sticholysin II from the sea anemone *Stichodactyla helianthus*, Eur J Biochem, 252 (1998) 284-289.

[27] C.A. Valcarcel, M. Dalla Serra, C. Potrich, I. Bernhart, M. Tejuca, D. Martínez, F. Pazos, M.E. Lanio, G. Menestrina, Effects of lipid composition on membrane permeabilization by sticholysin I and II, two cytolysins of the sea anemone *Stichodactyla helianthus*, Biophys J, 80 (2001) 2761-2774.

[28] D. Martínez, A. Otero, C. Álvarez, F. Pazos, M. Tejuca, M.E. Lanio, I. Gutiérrez-Aguirre, A. Barlič, I. Iloro, J.L. Arrondo, J.M. González-Mañas, E. Lissi, Effect of sphingomyelin and cholesterol on the interaction of St II with lipidic interfaces, Toxicon, 49 (2007) 68-81.

[29] B. Bakrač, G. Anderluh, Molecular mechanism of sphingomyelin-specific membrane binding and pore formation by actinoporins, Adv Exp Med Biol, 677 (2009) 106-115.

[30] S. García-Linares, J. Palacios-Ortega, T. Yasuda, M. Astrand, J.G. Gavilanes, A. Martínez-del-Pozo, J.P. Slotte, Toxin-induced pore formation is hindered by intermolecular hydrogen bonding in sphingomyelin bilayers, Biochim Biophys Acta, 1858 (2016) 1189-1195.

[31] S. García-Linares, E. Rivera-de-Torre, K. Morante, K. Tsumoto, J.M. Caaveiro, J.G. Gavilanes, J.P. Slotte, Á. Martínez-del-Pozo, Differential effect of membrane composition on the pore-forming ability of four different sea anemone actinoporins, Biochemistry, 55 (2016) 6630-6641.

[32] A.W. Bernheimer, L.S. Avigad, Properties of a toxin from the sea anemone *Stoichactis helianthus*, including specific binding to sphingomyelin, Proc Natl Acad Sci U S A, 73 (1976) 467-471.

[33] B. Bakrač, I. Gutierrez-Aguirre, Z. Podlesek, A.F. Sonnen, R.J. Gilbert, P. Maček, J.H. Lakey, G. Anderluh, Molecular determinants of sphingomyelin specificity of a eukaryotic pore-forming toxin, J Biol Chem, 283 (2008) 18665-18677.

[34] T. Maula, Y.J. Isaksson, S. García-Linares, S. Niinivehmas, O.T. Pentikainen, M. Kurita, S. Yamaguchi, T. Yamamoto, S. Katsumura, J.G. Gavilanes, A. Martínez-del-Pozo, J.P. Slotte, 2NH and 3OH are crucial structural requirements in sphingomyelin for sticholysin II binding and pore formation in bilayer membranes, Biochim Biophys Acta, 1828 (2013) 1390-1395.

[35] W. Varanda, A. Finkelstein, Ion and nonelectrolyte permeability properties of channels formed in planar lipid bilayer membranes by the cytolytic toxin from the sea anemone, *Stoichactis helianthus*, J Membr Biol, 55 (1980) 203-211.

[36] A. Barlič, I. Gutiérrez-Aguirre, J.M. Caaveiro, A. Cruz, M.B. Ruiz-Argüello, J. Pérez-Gil, J.M. González-Mañas, Lipid phase coexistence favors membrane insertion of equinatoxin-II, a pore-forming toxin from *Actinia equina*, J Biol Chem, 279 (2004) 34209-34216.

[37] J. Alegre-Cebollada, I. Rodríguez-Crespo, J.G. Gavilanes, A. Martínez-del-Pozo, Detergent-resistant membranes are platforms for actinoporin pore-forming activity on intact cells, FEBS J, 273 (2006) 863-871.

[38] J. Alegre-Cebollada, M. Cunietti, E. Herrero-Galán, J.G. Gavilanes, A. Martínez-del-Pozo, Calorimetric scrutiny of lipid binding by sticholysin II toxin mutants, J Mol Biol, 382 (2008) 920-930.

[39] M. Marchioretto, M. Podobnik, M. Dalla Serra, G. Anderluh, What planar lipid membranes tell us about the pore-forming activity of cholesterol-dependent cytolysins, Biophys Chem, 182 (2013) 64-70.

[40] L. Pedrera, M.L. Fanani, U. Ros, M.E. Lanio, B. Maggio, C. Álvarez, Sticholysin I-membrane interaction: an interplay between the presence of sphingomyelin and membrane fluidity, Biochim Biophys Acta, 1838 (2014) 1752-1759.

[41] L. Pedrera, A.B. Gomide, R.E. Sánchez, U. Ros, N. Wilke, F. Pazos, M.E. Lanio, R. Itri, M.L. Fanani, C. Álvarez, The presence of sterols favors sticholysin I-membrane association and pore formation regardless of their ability to form laterally segregated domains, Langmuir, 31 (2015) 9911-9923.

[42] I. Alm, S. García-Linares, J.G. Gavilanes, A. Martínez-del-Pozo, J.P. Slotte, Cholesterol stimulates and ceramide inhibits sticholysin II-induced pore formation in complex bilayer membranes, Biochim Biophys Acta - Biomembranes, 1848 (2015) 925-931.

[43] S. García-Linares, I. Alm, T. Maula, J.G. Gavilanes, J.P. Slotte, A. Martínez-del-Pozo, The effect of cholesterol on the long-range network of interactions established

among sea anemone Sticholysin II residues at the water-membrane interface, Mar Drugs, 13 (2015) 1647-1665.

[44] S. García-Linares, T. Maula, E. Rivera-de-Torre, J.G. Gavilanes, J.P. Slotte, A. Martínez-del-Pozo, Role of the tryptophan residues in the specific interaction of the sea anemone *Stichodactyla helianthus*'s actinoporin Sticholysin II with biological membranes, Biochemistry, 55 (2016) 6406-6420.

[45] E. Rivera-de-Torre, S. García-Linares, J. Alegre-Cebollada, J. Lacadena, J.G. Gavilanes, A. Martínez-del-Pozo, Synergistic action of actinoporin isoforms from the same sea anemone species assembled into functionally active heteropores, J Biol Chem, 291 (2016) 14109-14119.

[46] H.P. Wacklin, B.B. Bremec, M. Moulin, N. Rojko, M. Haertlein, T. Forsyth, G. Anderluh, R.S. Norton, Neutron reflection study of the interaction of the eukaryotic pore-forming actinoporin equinatoxin II with lipid membranes reveals intermediate states in pore formation, Biochim Biophys Acta, 1858 (2016) 640-652.

[47] J. Palacios-Ortega, S. García-Linares, E. Rivera-de-Torre, J.G. Gavilanes, A. Martínez-del-Pozo, J.P. Slotte, Sticholysin, Sphingomyelin, and Cholesterol: A Closer Look at a Tripartite Interaction, Biophys J, 116 (2019) 2253-2265.

[48] D. Suput, Effects of Equinatoxin on the Membrane of Skeletal-Muscle Fiber, Period Biol, 88 (1986) 210-211.

[49] R. Zorec, M. Tester, P. Maček, W.T. Mason, Cytotoxicity of equinatoxin II from the sea anemone *Actinia equina* involves ion channel formation and an increase in intracellular calcium activity, J Membr Biol, 118 (1990) 243-249.

[50] P. Maček, Polypeptide cytolytic toxins from sea anemones (Actiniaria), FEMS Microbiol Immunol, 5 (1992) 121-129.

[51] P. Maček, G. Belmonte, C. Pederzolli, G. Menestrina, Mechanism of action of equinatoxin II, a cytolysin from the sea anemone *Actinia equina* L. belonging to the family of actinoporins, Toxicology, 87 (1994) 205-227.

[52] C. Alvarez, F. Casallanovo, C.S. Shida, L.V. Nogueira, D. Martínez, M. Tejuca, I.F. Pazos, M.E. Lanio, G. Menestrina, E. Lissi, S. Schreier, Binding of sea anemone pore-forming toxins sticholysins I and II to interfaces-Modulation of conformation and activity, and lipid-protein interaction, Chem Phys Lipids, 122 (2003) 97-105.

[53] J. Alegre-Cebollada, G. Clementi, M. Cunietti, C. Porres, M. Oñaderra, J.G. Gavilanes, A. Martínez-del-Pozo, Silent mutations at the 5'-end of the cDNA of actinoporins from the sea anemone *Stichodactyla helianthus* allow their heterologous overproduction in *Escherichia coli*, J Biotechnol, 127 (2007) 211-221.

[54] S. García-Linares, R. Richmond, M.F. García-Mayoral, N. Bustamante, M. Bruix, J.G. Gavilanes, A. Martínez-del-Pozo, The sea anemone actinoporin (Arg-Gly-Asp) conserved motif is involved in maintaining the competent oligomerization state of these pore-forming toxins, FEBS J, 281 (2014) 1465-1478.

[55] J.M. Rausch, W.C. Wimley, A high-throughput screen for identifying transmembrane pore-forming peptides, Anal Biochem, 293 (2001) 258-263.

[56] W.C. Wimley, Determining the Effects of Membrane-Interacting Peptides on Membrane Integrity, Methods Mol Biol, 1324 (2015) 89-106.

[57] J. Wilschut, D. Papahadjopoulos, Ca^{2+}-induced fusion of phospholipid vesicles monitored by mixing of aqueous contents, Nature, 281 (1979) 690-692.

[58] A. Andersson, J. Danielsson, A. Graslund, L. Maler, Kinetic models for peptide-induced leakage from vesicles and cells, Eur Biophys J, 36 (2007) 621-635.

[59] P. Maček, M. Zecchini, C. Pederzolli, M. Dalla Serra, G. Menestrina, Intrinsic tryptophan fluorescence of equinatoxin II, a pore- forming polypeptide from the sea anemone *Actinia equina* L, monitors its interaction with lipid membranes, Eur J Biochem, 234 (1995) 329-335.

[60] X. Jiang, H. Chen, W. Yang, Y. Liu, W. Liu, J. Wei, H. Tu, X. Xie, L. Wang, A. Xu, Functional expression and characterization of an acidic actinoporin from sea anemone *Sagartia rosea*, Biochem Biophys Res Commun, 312 (2003) 562-570.

[61] M. Ahumada, C. Calderon, E. Lissi, C. Alvarez, M.E. Lanio, F. Pazos, The pore forming capacity of Sticholysin I in dipalmitoyl phosphatidyl vesicles is tuned by osmotic stress, Chem Phys Lipids, 203 (2017) 87-93.

[62] G.P.B. Carretero, E.F. Vicente, E.M. Cilli, C.M. Alvarez, H. Jenssen, S. Schreier, Dissecting the mechanism of action of actinoporins. Role of the N-terminal amphipathic alpha-helix in membrane binding and pore activity of sticholysins I and II, PLoS One, 13 (2018) e0202981.

[63] C. Soto, A. Del Valle, P.A. Valiente, U. Ros, M.E. Lanio, A.M. Hernandez, C. Alvarez, Differential binding and activity of the pore-forming toxin sticholysin II in model membranes containing diverse ceramide-derived lipids, Biochimie, 138 (2017) 20-31.

[64] U. Ros, G.P.B. Carretero, J. Paulino, E. Crusca, Jr., F. Pazos, E.M. Cilli, M.E. Lanio, S. Schreier, C. Alvarez, Self-association and folding in membrane determine the mode of action of peptides from the lytic segment of sticholysins, Biochimie, 156 (2019) 109-117.

[65] H. Mesa-Galloso, K.H. Delgado-Magnero, S. Cabezas, A. Lopez-Castilla, J.E. Hernandez-Gonzalez, L. Pedrera, C. Alvarez, D. Peter Tieleman, A.J. Garcia-Saez, M.E. Lanio, U. Ros, P.A. Valiente, Disrupting a key hydrophobic pair in the oligomerization interface of the actinoporins impairs their pore-forming activity, Protein Sci, 26 (2017) 550-565.

[66] R.J. Laborde, O. Sanchez-Ferras, M.C. Luzardo, Y. Cruz-Leal, A. Fernandez, C. Mesa, L. Oliver, L. Canet, L. Abreu-Butin, C.V. Nogueira, M. Tejuca, F. Pazos, C. Alvarez, M.E. Alonso, I.M. Longo-Maugeri, M.N. Starnbach, D.E. Higgins, L.E. Fernandez, M.E. Lanio, Novel Adjuvant Based on the Pore-Forming Protein Sticholysin II Encapsulated into Liposomes Effectively Enhances the Antigen-Specific CTL-Mediated Immune Response, J Immunol, 198 (2017) 2772-2784.

[67] Y. Tamba, H. Ariyama, V. Levadny, M. Yamazaki, Kinetic pathway of antimicrobial peptide magainin 2-induced pore formation in lipid membranes, J Phys Chem B, 114 (2010) 12018-12026.

[68] M.B. Mustafa, D.L. Tipton, M.D. Barkley, P.S. Russo, F.D. Blum, Dye Diffusion in Isotropic and Liquid-Crystalline Aqueous (Hydroxypropyl)Cellulose, Macromolecules, 26 (1993) 370-378.

[69] J. Martín-Benito, F. Gavilanes, V. de Los Ríos, J.M. Mancheño, J.J. Fernández, J.G. Gavilanes, Two-dimensional crystallization on lipid monolayers and three-dimensional structure of sticholysin II, a cytolysin from the sea anemone *Stichodactyla helianthus*, Biophys J, 78 (2000) 3186-3194.

[70] R. Peters, Fluorescence microphotolysis to measure nucleocytoplasmic transport and intracellular mobility, Biochim Biophys Acta, 864 (1986) 305-359.

[71] C.B. Muller, A. Loman, V. Pacheco, F. Koberling, D. Willbold, W. Richtering, J. Enderlein, Precise measurement of diffusion by multi-color dual-focus fluorescence correlation spectroscopy, Epl-Europhys Lett, 83 (2008) 46001.

[72] M.A. Baker, N. Rojko, B. Cronin, G. Anderluh, M.I. Wallace, Photobleaching Reveals Heterogeneous Stoichiometry for Equinatoxin II Oligomers, Chembiochem, 15 (2014) 2139-2145.

[73] K. Tanaka, J.M. Caaveiro, K. Tsumoto, Bidirectional Transformation of a Metamorphic Protein between the Water-Soluble and Transmembrane Native States, Biochemistry, 54 (2015) 6863-6866.

[74] J. Alegre-Cebollada, A. Martínez-del-Pozo, J.G. Gavilanes, E. Goormaghtigh, Infrared spectroscopy study on the conformational changes leading to pore formation of the toxin sticholysin II, Biophys J, 93 (2007) 3191-3201.

[75] K.C. Kristan, G. Viero, M. Dalla Serra, P. Maček, G. Anderluh, Molecular mechanism of pore formation by actinoporins, Toxicon, 54 (2009) 1125-1134.

[76] Y. Subburaj, U. Ros, E. Hermann, R. Tong, A.J. García-Sáez, Toxicity of an α-pore-forming toxin depends on the assembly mechanism on the target membrane as revealed by single-molecule imaging, J Biol Chem, 290 (2015) 4856-4865.

[77] K. Cosentino, U. Ros, A.J. García-Sáez, Assembling the puzzle: Oligomerization of α-pore forming proteins in membranes, Biochim Biophys Acta, 1858 (2016) 457-466.

[78] K. Morante, A. Bellomio, D. Gil-Carton, L. Redondo-Morata, J. Sot, S. Scheuring, M. Valle, J.M. Gonzalez-Manas, K. Tsumoto, J.M.M. Caaveiro, Identification of a Membrane-bound Prepore Species Clarifies the Lytic Mechanism of Actinoporins, Journal of Biological Chemistry, 291 (2016) 19210-19219.

[79] A.J. Krauson, J. He, W.C. Wimley, Determining the mechanism of membrane permeabilizing peptides: identification of potent, equilibrium pore-formers, Biochim Biophys Acta, 1818 (2012) 1625-1632.

[80] A.J. Krauson, J. He, W.C. Wimley, Gain-of-function analogues of the pore-forming peptide melittin selected by orthogonal high-throughput screening, J Am Chem Soc, 134 (2012) 12732-12741.

[81] Y. Marcus, Volumes of aqueous hydrogen and hydroxide ions at 0 to 200ºC, J Chem Phys, 137 (2012) 154501.

[82] E.F. Pettersen, T.D. Goddard, C.C. Huang, G.S. Couch, D.M. Greenblatt, E.C. Meng, T.E. Ferrin, UCSF Chimera--a visualization system for exploratory research and analysis, J Comput Chem, 25 (2004) 1605-1612.

Table 1.

Parameters obtained from each leakage assay.

Assay	LC_{50} (nM)	Release rate at 20 nM ($\Delta F \cdot s^{-1}$)	Saturation (% of release)
Calcein	0.052	0.061	53.2
R6G	0.009	0.235	53.5
Tb^{3+}	1.990	0.051	55.1
H^{+} (Fluorescein)	2.880	0.201	62.5

Table 2.

Estimated ionic radius for the different ions or fluorescence probes used in this and other studies.

Ion	*Calcein*	*Rhodamine 6G*	*Carboxyfluorescein*	*Terbium*	*H^+*	*Dithionite*	*Potassium*	*Calcium*	*NADH*	*dextran FD-4*
Estimated radius (nm)	0.74	0.59	0.50	0.12	0.10[a]	0.20[b]	0.14	0.10	0.60	1.40

[a] [81]

[b] Estimated approximate value for dithionite ($S_2O_4^{2-}$). For comparison, SO_4^{2-} ionic radius is 0.26 nm.

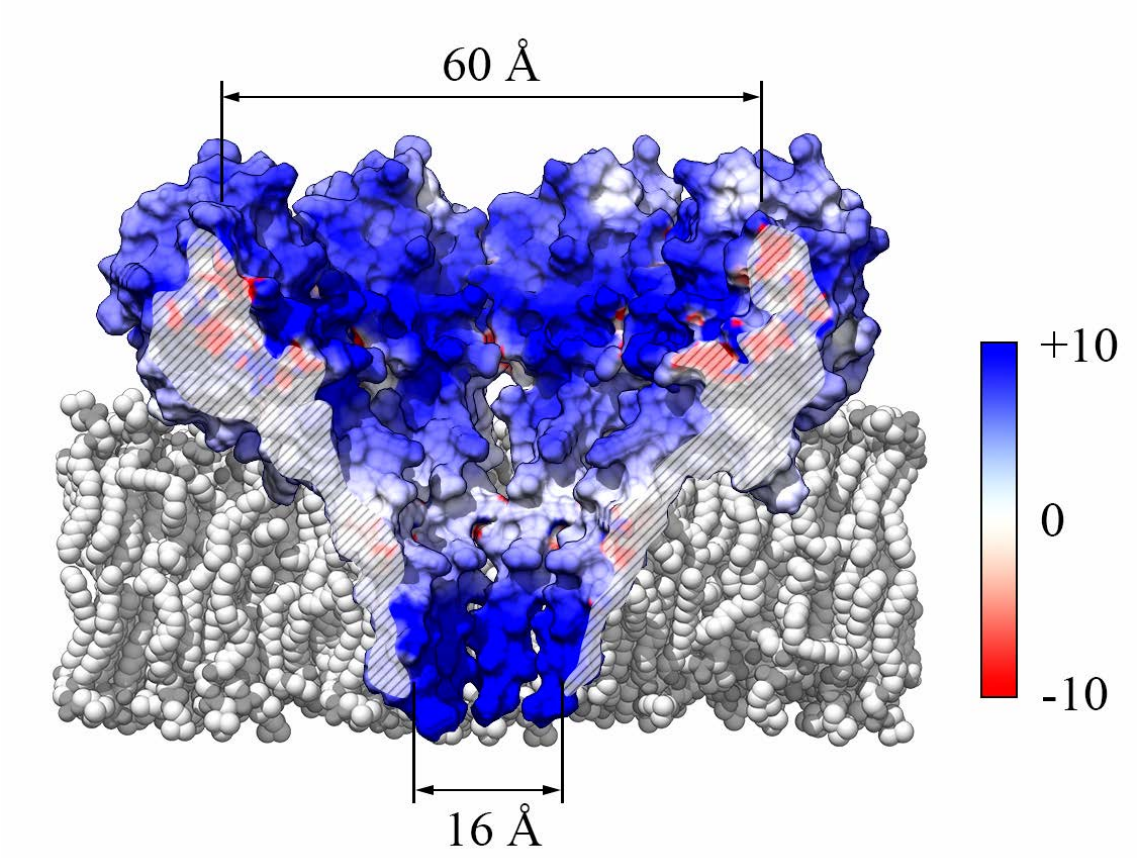

Fig. 1. Three-dimensional structure of the crystalline octameric pore of the actinoporin sticholysin II, obtained by fitting StnII monomeric structure (PDB ID: 1GWY) to the octameric pore structure of fragaceatoxin C obtained in presence of detergents (PDB ID: 4TSY) [15]. The helix was constructed based on the known sequence of StnII and fitting it to the same structure. The pore has a narrowest constriction of ~16 Å in its cytoplasmic side, opening to ~60 Å in its upper vestibule. Surface was coloured according to the electrostatic potential in the protein, as calculated using APBS *via* the UCSF Chimera software [82]. The protein was prepared for APBS using the PDB2PQR tool *via* UCSF Chimera as well. Units are k_BT/e_c. Striped areas on the sides of the pore are used to outline the lumen of the pore, and enclose, approximately, the surfaces of monomer-monomer contacts as well as voids that seem to be occupied by lipids [15].

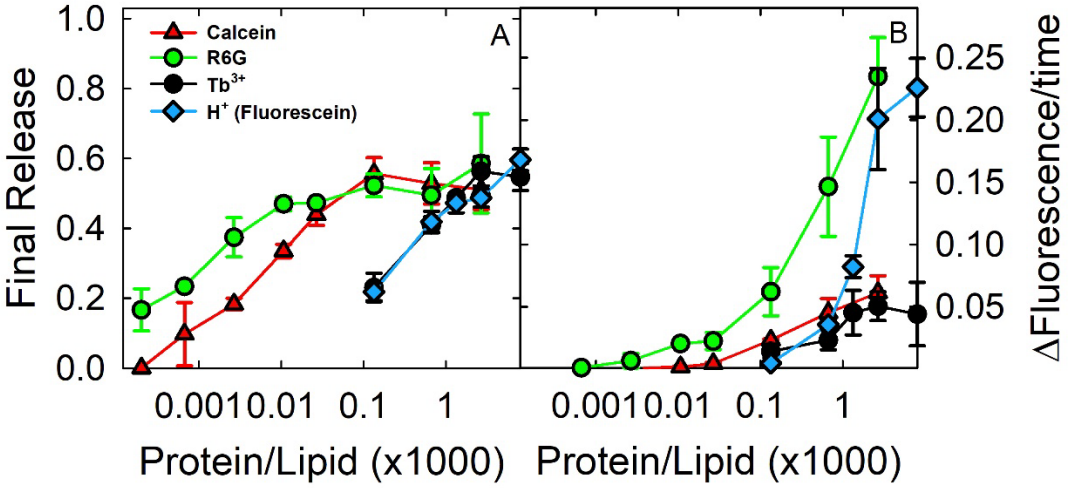

Fig. 2. Leakage experiments. (A) Percentages of final release after 5 min and (B) maximal rates of leakage of different molecules or ions entrapped in DOPC/SM/Chol (1:1:1) vesicles by StnII at different protein/lipid molar ratios. The ions used were calcein (red), rhodamine 6G (green), Tb^{3+}:citrate (black), and H^{+} (fluorescein) (blue). Release was measured at 23 °C. All intensities were normalized. At the end of the measurement, a suitable detergent was added to dissolve the LUVs and obtain 100 % of release. The results shown are representative of two or three different independent experiments. Each value is the average ± SEM.

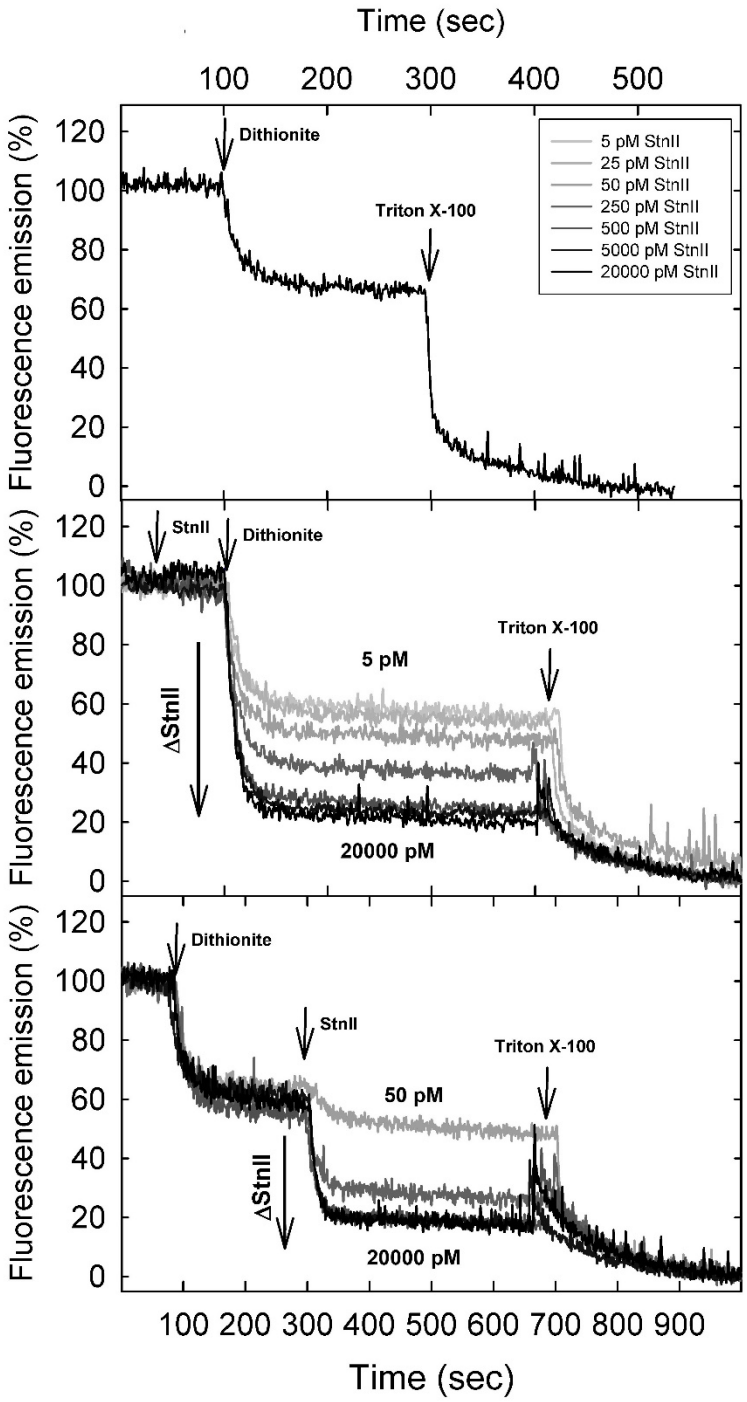

Fig. 3. Equilibrium pore assays. Sodium dithionite was added (final concentration 55 mM) to DOPC:eSM:Chol (1:1:1) LUVs containing 1 mol% of POPE-NBD. (A) The vesicles were first incubated with dithionite, and then were completely disintegrated by the addition of Triton X-100 to a final concentration of 0.045 % v/v. (B) Same as in (A) but the vesicles were previously incubated with increasing concentrations of StnII. (C) Dithionite was added first, then the actinoporin StnII and, finally, the remaining vesicles were also disintegrated with Triton X-100. The protein concentrations employed were 5 pM, 25 pM, 50 pM, 250 pM, 0.5 nM, 5 nM and 20 nM.

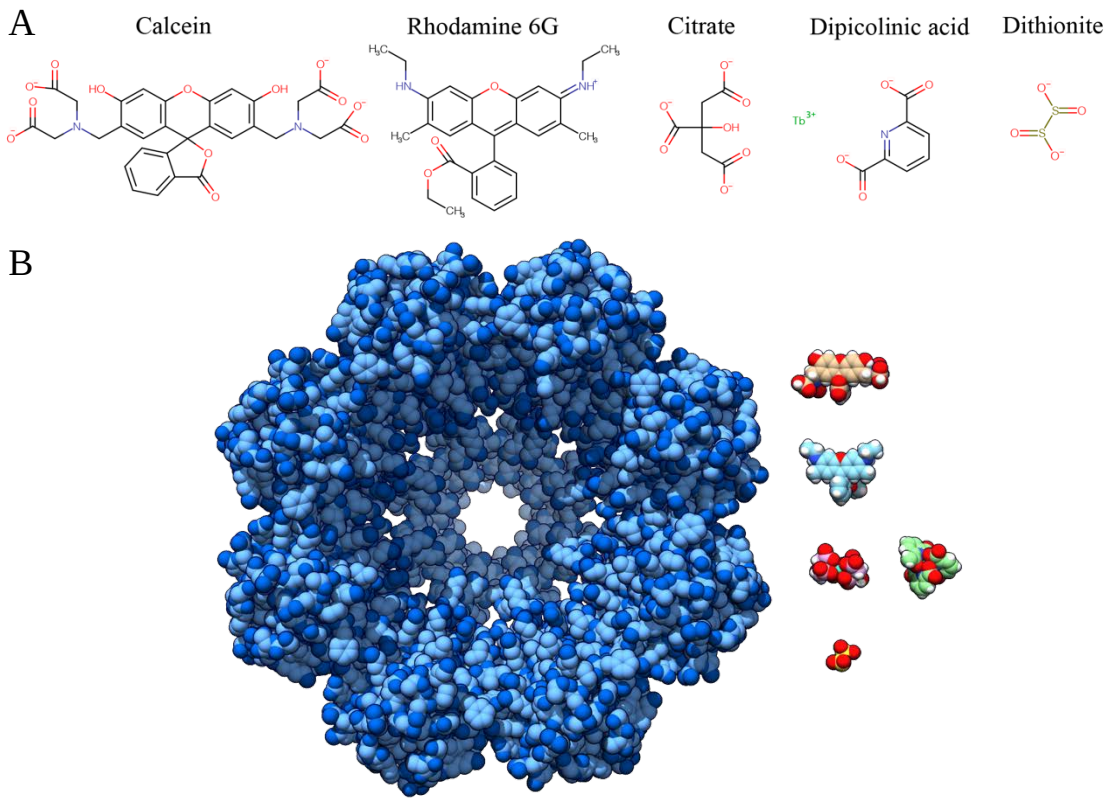

Fig. 4. (A) Chemical structures of the molecules used in this work to estimate release rates and extent through actinoporins' pores. Formula weights of the molecules and the complexes they form are: Calcein (FW 623), Rhodamine 6G (FW 479), Tb^{3+} (FW 160) in complex with two molecules of citrate (FW 189; FW of the complex 543, in practice, size is that of a ~400 Da complex), Tb^{3+} in complex with three molecules of DPA (FW 165; FW of the complex 654, in practice, size is that of a ~510 Da complex), and dithionite (FW 174). Proton is omitted in the figure. (B) Cartoon illustrating the relative size of the complexes shown above, as compared to the StnII pore from Fig. 1, using CPK representation. Tb^{3+} is shown in a 1:2 complex with citrate (pink) and a 1:3 complex with DPA (light green). Formulas were made using the Marvin 19.22 (2019) software from ChemAxon. Three-dimensional representations are rendered using UCSF Chimera [82].

Figure S1

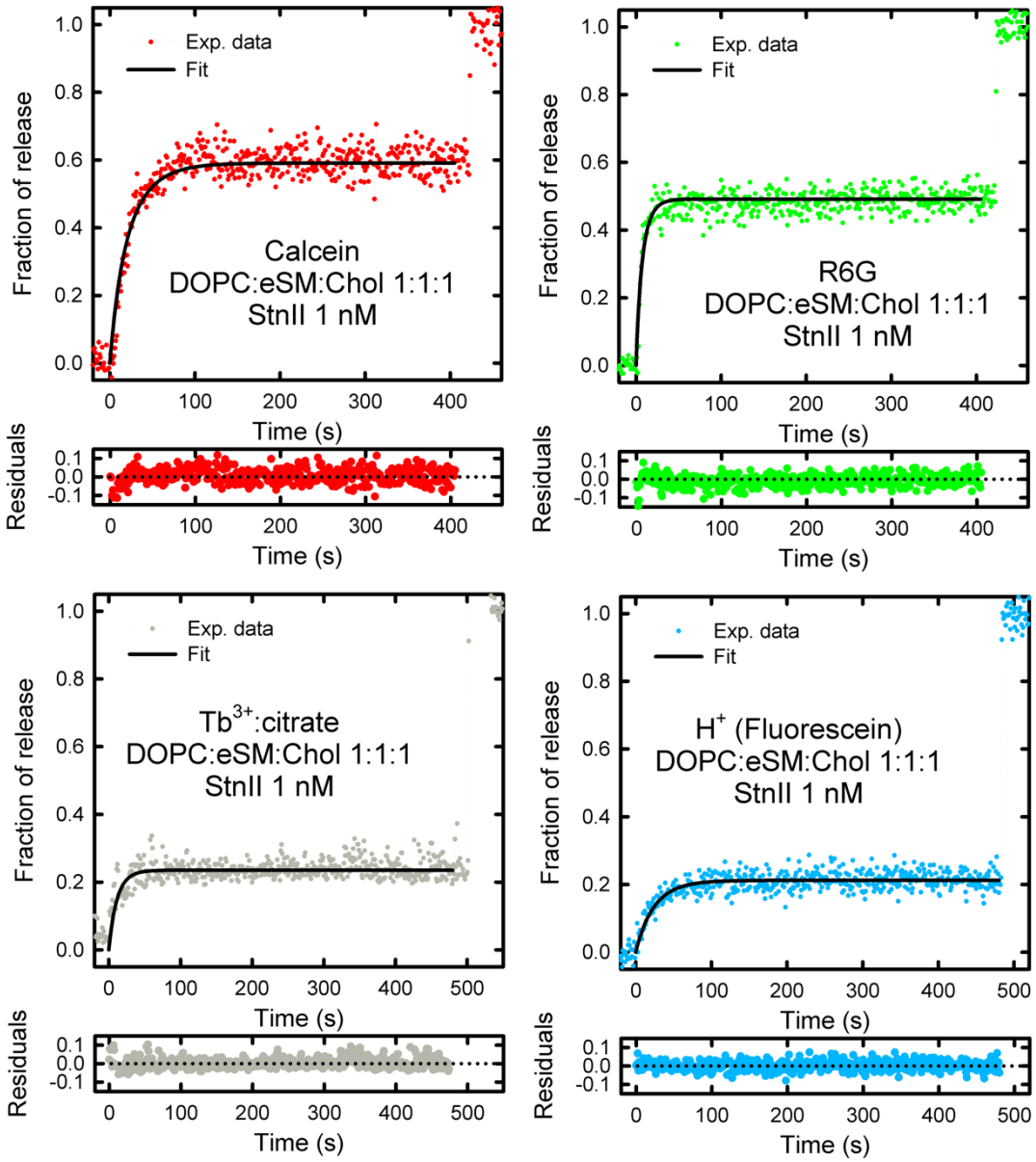

Fig. S1. Representative experimental data from calcein (red), R6G (green), Tb^{3+}:citrate (grey), and H^+ (fluorescein) (blue) release from LUVs. In black solid lines the fits to each trace of the perturbation model are shown. Small panels show the residuals of each fit.

Graphical Abstract (TOC)